Photodetachment of the $1s2s2p\ ^4P$ state of He^- from threshold to 100 eV

Dae-Soung Kim,* Hsaio-Ling Zhou, and Steven T. Manson
Department of Physics and Astronomy, Georgia State University, Atlanta, Georgia 30303
(Received 19 June 1996)

Calculations of cross sections and photoelectron angular distributions from the photodetachment of the $1s2s2p\ ^4P$ metastable state of He^- have been performed from threshold to 100 eV using multiconfiguration Hartree-Fock wave functions for discrete states and coupling continuum channels with closed channels to include resonances. Ejection of each electron was considered and ejection plus excitation was included in connection with $1s$ photoabsorption. The $1s2p^2$ and $2s2p^2\ ^4P$ resonances were found in good agreement with recent experiments and calculations; the reason that the former lies above the $2s$ threshold while the latter lies below the $1s$ threshold is discussed. The nonresonant $2p$ cross section is in excellent agreement with experiments and other calculations. The $2s$ results, in which Cooper minima are predicted, are not in agreement with a similar calculation, particularly for the β parameter. The $1s$ cross section shows a large maximum just above threshold, much larger than the $1s$ cross section in neutral He, and at somewhat higher energy the cross section is dominated by $1s$ detachment plus excitation to the $(2s3p \pm 3s2p)\ ^3P$ and $3s3p\ ^3P$ autoionizing states of He. [S1050-2947(97)06801-7]

PACS number(s): 32.80.Gc, 32.80.Hd, 32.80.Dz

I. INTRODUCTION

The absorption of photons by atoms and ions is a fundamental process of nature as well as being of applied importance in many other areas of physics and technology [1]. Consequently, over the past three decades, a great deal has been done in this area and much of the general phenonmenology of the photoionization of neutral atoms and positive ions is known [2–5]. In these cases, the influence of correlation is important but not generally dominant. The situation is otherwise for negative ions where correlation is much more important. Thus photodetachment of negative ions is an excellent ''laboratory'' in which to emphasize the effects of correlation.

In this paper, an investigation of the photodetachment of the $1s2s2p\ ^4P$ state of He^- is presented. We have considered detachment of the outer $2s$ and $2p$ electrons, as well as, the inner $1s$ in order to get some feeling for how the effects of correlation might differ in outer vs inner shells. This state of He^- was chosen for several reasons. The $j=5/2$ fine-structure component is metastable, with a lifetime of the order of 0.5 ms [6], so it lives long enough to be amenable for experimental investigation. Second, there have been a number of recent experimental [7–13] and theoretical [14–22] investigations of this photodetachment process and the resonances associated with it. Third, and most important, the $1s2s2p\ ^4P$ state of He^- is a very highly correlated system; without introducing correlation the system is not bound. Thus, correlation is not a small perturbation on the system, it is a dominant determinant of the behavior of the system. Our primary interest is how the various aspects of correlation translate into the behavior of dynamical observables, photodetachment cross sections, and photoelectron angular distribution asymmetry, β, parameters. To that end we have considered correlation in the various initial and final discrete states via multiconfiguration Hartree-Fock (MCHF) wave functions [23], as well as coupling between open and closed channels which are responsible for resonances; we have excluded coupling between open channels here. This means that interactions are omitted which can substantially alter the cross sections of weak channels degenerate with strong ones. But this limitation will not affect strong channels appreciably. In addition, we have included not only ejection of each of the electrons, but also investigated a large energy range, from threshold to a photon energy of 100 eV. Since our interest is a study over a broad energy range, we have omitted from the calculation valence shell detachment plus excitation; this omission should not be important except in the small photon energy region from about 3–5 eV.

In Sec. II, a discussion of the theory and our theoretical methodology is presented. In Sec. III, our results are presented, discussed, and compared with other theoretical and experimental work. Section IV presents a summary and conclusions.

II. THEORY AND CALCULATIONAL DETAILS

Within the framework of the electric dipole approximation, which is excellent for low-energy photoabsorption processes, the cross section for a transition from initial state i to final state f via absorption of a photon of energy $\hbar\omega$, is given by [2]

$$\sigma_{if}=\frac{4\pi^2\omega}{g_i c}\left|\vec{\varepsilon}\cdot\left\langle\psi_i\left|\sum\vec{r}_j\right|\psi_f\right\rangle\right|^2, \tag{1}$$

where g_i is the multiplicity of the initial state, c is the speed of light, and ε is the photon polarization. In Eq. (1) summing over final, and averaging over initial, magnetic substates is implied. Equation (1) is given in the so-called length formulation; alternate forms of the transition matrix element [24], known as velocity or acceleration forms, which yield identi-

*Present address: Department of Physics, Myong-Ji University, Yong-In, Kyungki 449-738, Korea.

 © 1997 The American Physical Society

TABLE I. MCHF expansion coefficients for the $1s2s2p\ ^4P$ State of He^-.

Configuration	Coefficient
$1s2s2p$	0.861 622 2
$1s2s3p$	0.447 856 7
$1s3s2p$	−0.122 045 4
$1s2p3d$	−0.168 642 9
$1s3s3p$	0.082 403 6
$1s2s4p$	−0.047 438 8
$1s2s5p$	−0.059 389 8
$1s3s5p$	−0.013 786 9
$1s3d5p$	−0.013 297 5

cal results for exact wave functions, exist and these are useful as indicators of the quality of the wave functions employed. The wave functions themselves are discussed below.

The differential cross section for photodetachment or photoionization in the dipole approximation is given by [25]

$$\frac{d\sigma_{if}}{d\Omega} = \frac{\sigma_{if}}{4\pi}\,[1+\beta_{if}P_2(\cos\theta)], \tag{2}$$

where θ is the angle between the photon polarization and photoelectron direction, $P_2(x)=(3x^2-1)/2$, and β_{if} is the photoelectron angular distribution asymmetry parameter; its detailed formulation is given elsewhere [26]. Suffice it to say that it depends upon the matrix elements and their phases for the various channels leading to a given final core state.

The wave functions for the all bound states, and quasibound resonance states, employed in this work were obtained using multiconfiguration Hartree-Fock (MCHF) wave functions [27]; linear combinations of determinental (single configuration) wave functions comprised of antisymmetrized products of single-particle orbitals, where the radial parts of each single-particle orbital is varied along with the coefficient of each configuration. He^- in the $1s2s2p\ ^4P$ state is a particularly highly correlated system, in that it is not even bound at the HF level of approximation. As an indicator of the accuracy of the bound-state wave functions employed, the ground state can be scrutinized. The principal terms in the MCHF wave function, i.e., the terms with the largest coefficients, are shown in Table I. It is clear form this table that, although the $1s2s2p$ configuration is the most important, others are important as well, notably $1s2s3p$, $1s2p3s$, and $1s2p3d$. It should be noted that, except for the orbitals included in the main configuration, the other orbitals are correlation orbitals and are not necessarily related to the ''physical'' orbitals of the same designation. We used a total of 162 configurations in the energy calculation and obtained −2.177 991 7 a.u. for the total energy of the $1s2s2p\ ^4P$ state of He^-. This compares with the best previous theoretical value [28] of −2.178 077 6 a.u., a difference of about 2 meV.

The $1s2s\ ^3S$ state of neutral He is well described even at the HF level. We used a MCHF function including all configurations up to $n=3$ (going to higher n gave nothing appreciable), and obtained an energy of −2.175 218 3 a.u., a difference of only about 0.3 meV from the experimental value of −2.175 229 4 a.u. [29]. Aside from the main configuration, only $2p3p$ (0.0190) has a coefficient >0.005. Thus our purely theoretical binding energy of the $1s2s2p\ ^4P$ state of He^- is 75.5 meV which compares reasonably with the best experimental value [13] of 77.67±0.12 meV. Similarly, the $1s2p\ ^3S$ state is nearly HF, with slight admixtures of $2s3p$ and $2p3d$ and nothing else with coefficient >0.005. We obtained an energy of −2.133 09 a.u., in excellent agreement with −2.133 17 a.u. of experiment [29].

The doubly excited triplet final states of He present more of a problem because there are no experimental values with which to compare them; nevertheless accurate theoretical values exist [30]. For the $2s2p\ ^3P$ state of He, our MCHF calculation, including all configurations up to $n=5$, and insuring orthogonality to lower states of the same symmetry, shows noticeable admixtures with $2s3p$, $2p3s$, and $2p4d$, all with coefficients >0.1. The energy obtained was −0.7601 a.u., in rather good agreement with the best theoretical value of −0.7614 a.u. [30]. The MCHF results for the $(2s3p\pm3s2p)\ ^3P$ states of He show, in addition to the complete mixing of $2s3p$ and $2p3s$ configurations, reasonable strong mixing with $2s2p$, $2p3d$, and $2p4d$ as well. Our energies of −0.5840 a.u. and −0.5762 a.u. compare well with the best theoretical numbers, −0.5849 a.u. and −0.5790 a.u., respectively [30]. Finally, for the $3s3p\ ^3P$ state, $3s3p$ and $3p3d$ are strongly admixed with coefficients 0.92 and 0.38, respectively, with $4s4p$ (0.03) being the only other non-negligible contribution, giving −0.3499 a.u., in excellent agreement with the −0.3508 a.u. of previous theory [31]. In summary, the bound-state energies, and thereby, the thresholds used in the calculation are rather accurate; this suggests that the bound-state wave functions are also of significant accuracy.

Final continuum states in the nonresonant region are taken single channel HF, but in the MCHF field of the core obtained using our own codes [32]. This procedure, neglecting interchannel coupling, is justified as long as we are scrutinizing the total cross section, which is dominated in each energy range by a single channel of each symmetry. Thus, while interchannel coupling can have a significant effect on weak channels degenerate with strong ones, it has only minor influence upon the dominant channels. In the vicinity of a resonance, however, there is then more than one strong channel, so the interaction between the resonance and the continuum channel must be included.

Two resonances, $1s2p^2\ ^4P$ and $2s2p^2\ ^4P$, were included in this calculation; they are represented by MCHF [27] wave functions of 95 and 57 configurations, respectively. The former contained all terms with coefficients $>10^{-5}$ up to $n=4$, and the latter up to $n=5$. While the main configuration dominated in both cases, much correlation still exists. Using these discrete wave functions, along with the continuum wave functions of the same symmetry (described above), a Fano continuum configuration interaction calculation [33] was performed and the resulting final-state wave function is used to obtain the dipole matrix element, again using our own codes. Implicit in this resonance calculation, the width of each resonance is obtained. The agreement of our resonance results with experiments and other calculations, discussed below, suggests that our calculation treats the resonances reasonably accurately.

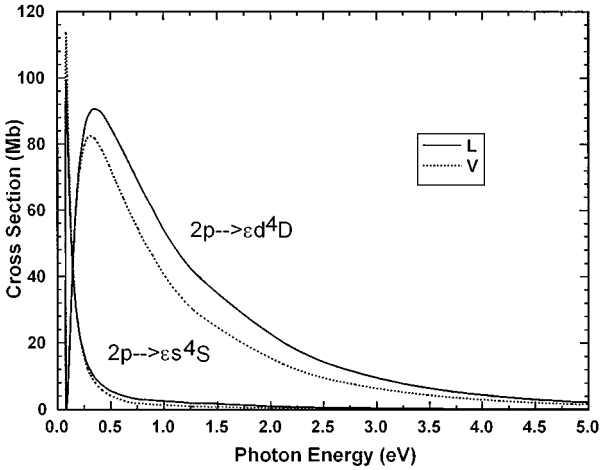

FIG. 1. Calculated $1s2s2p\ ^4P \rightarrow 1s2s\varepsilon s\ ^4S$ and $1s2s\varepsilon d\ ^4D$ partial photodetachment cross sections in He^- in dipole-length (L) and dipole-velocity (V) formulations.

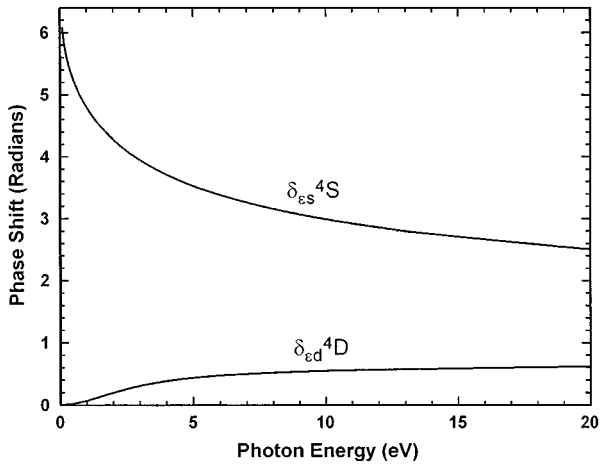

FIG. 2. Phase shifts for the $1s2s\varepsilon s\ ^4S$ and $1s2s\varepsilon d\ ^4D$ final continuum states in He^-.

This methodology, where initial and final states are calculated variationally and independently from one another, has an important advantage; most states can be well described by a small number of terms in the MCHF expansion so that the physics included in the calculation, in both initial and final states, is relatively easy to pick out. This, in turn, leads to a relatively small number of combinations of initial and final configurations contributing to the dipole matrix element, so that the effects are various terms in the wave function on the photoionization process can be sorted out. On the negative side, however, the lack of orthogonality between the single-particle wave functions in the initial and final states leads to greater complexity in the calculation of each term in the dipole matrix element.

III. RESULTS AND DISCUSSION

A. Photodetachment of the $2p$ electron: The $1s2s\ ^3S$ He channel

Using the methodology described above, the $2p$ cross section, leading to the $1s2s\ ^3S$ state of He was calculated; this cross section is the sum of the $1s2s2p\ ^4P \rightarrow 1s2s\varepsilon s\ ^4S$ and $1s2s\varepsilon d\ ^4D$ partial cross sections which are shown individually in Fig. 1, where it is seen that both partial cross sections vanish at threshold (which photodetachment cross sections must), they behave rather differently otherwise. The $p \rightarrow s$, ^4S, cross section increases very rapidly from threshold to its maximum of about 100 Mb around 0.0005 Ry above threshold, and then rapidly decreases with increasing energy. The $p \rightarrow d$, ^4D, cross section also has a maximum of about 100 Mb, but this maximum is seen to be considerably further above threshold than in the ^4S case, and the decline from the maximum, with increasing energy, is also seen to be much more gradual.

To understand this behavior, we first note that although we employed MCHF wave functions in the calculation, the dipole matrix elements for $2p$ detachment are dominated by contributions from two initial state and one final-state configuration, i.e., to a reasonably good approximation, the matrix elements can be characterized as

$$M(^4S) = \alpha_1 \langle 1s_i 2s_i 2p_i\ ^4P | D | 1s_f 2s_f \varepsilon s\ ^4S \rangle + \alpha_2 \langle 1s_i 2s_i 3p_i\ ^4P | D | 1s_f 2s_f \varepsilon s\ ^4S \rangle, \quad (3)$$

and

$$M(^4D) = \alpha_1 \langle 1s_i 2s_i 2p_i\ ^4P | D | 1s_f 2s_f \varepsilon d\ ^4D \rangle + \alpha_2 \langle 1s_i 2s_i 3p_i\ ^4P | D | 1s_f 2s_f \varepsilon d\ ^4D \rangle, \quad (4)$$

where D represents the dipole operator, the subscripts i and f emphasize that the initial- and final-state orbitals are different, i.e., core relaxation is included, and the α_i are the MCHF mixing coefficients of the initial state (from Table I), $\alpha_1 = 0.861\,62$ and $\alpha_2 = 0.447\,86$. Thus, aside from overlap and angular factors, these matrix elements are determined from the single-particle matrix elements between the discrete orbitals $2p_i$ and $3p_i$, and the continuum εs and εd. The matrix elements depend, therefore, upon the details of the εs and εd continuum wave functions.

Continuum wave functions can be characterized by their phase shifts; these are shown in Fig. 2 where it is seen that $\delta_{\varepsilon s}$ is 2π at threshold and decreases with increasing energy, while $\delta_{\varepsilon d}$ is zero at threshold and increases slowly with energy. Thus, the εs is very penetrating, at low energies, into the region of space occupied by the initial state, while the εd is not. Furthermore, the amplitude of the εs in the inner region increases as $\varepsilon^{1/2}$, while for the εd, the dependence is $\varepsilon^{3/2}$; this is due to the existence of the centrifugal barrier in the εd case which makes the penetration of εd into the interior region require more energy than εs. This is why $M(^4S)$ increases much more rapidly from threshold than $M(^4D)$, thereby reaching its maximum value much closer to threshold.

At energies much above the maximum in $M(^4S)$, the εs penetrates enough so that its oscillations in the inner region cause cancellation, thus the decrease. The same general behavior occurs for $M(^4D)$, but the maximum occurs at much higher energy, as discussed, and the falloff from the maximum, with increasing energy, occurs much more slowly than in the ^4S case, owing to the centrifugal barrier which causes the εd to penetrate more slowly than the εs with energy.

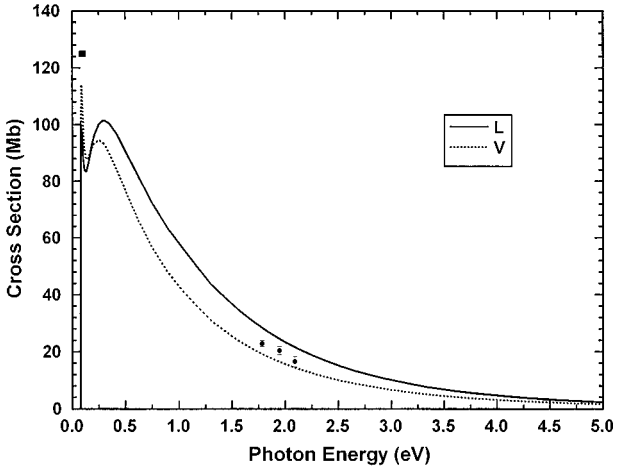

FIG. 3. Total $1s2s2p\ ^4P \rightarrow 1s2s\ ^3S$ photodetachment cross section, the sum of $\sigma(^4S)$ and $\sigma(^4D)$, in dipole-length (L) and dipole-velocity (V) formulations. The points with error bars are the experimental results of Refs. [7] and [11], while the low-energy point is the experimental result of Ref. [8].

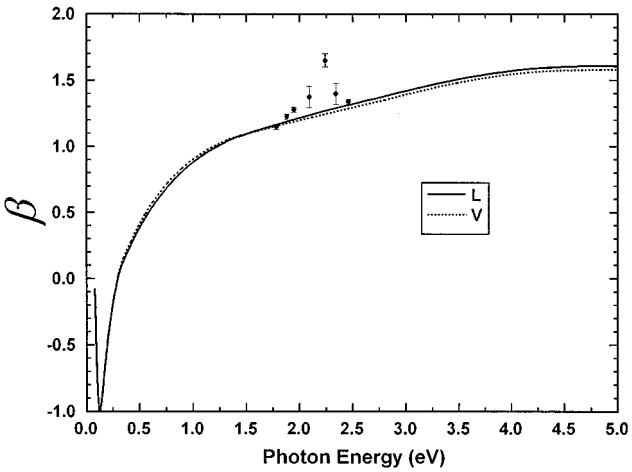

FIG. 4. Photoelectron angular distribution asymmetry parameter, β, for the $1s2s2p\ ^4P \rightarrow 1s2s\ ^3S$ photodetachment process in dipole-length (L) and dipole-velocity (V) formulations. The experimental points are from Refs. [11] and [12].

In Fig. 1 both length and velocity results for $\sigma(^4S)$ and $\sigma(^4D)$ are shown. The rather good agreement between them, within 15% over the entire energy range, suggests that the wave functions, discrete and continuum, employed in this calculation are reasonably accurate.

The total $1s2s2p\ ^4P \rightarrow 1s2s\ ^3S$ cross section, the sum of $\sigma(^4S)$ and $\sigma(^4D)$, is shown in Fig. 3, where the ^4S and ^4D maxima are seen. Also shown are the experimental results [7,8,11] which are in good agreement with the calculations. Not shown in the figure are the earlier theoretical results [18] which are also in substantial agreement with the present results. Thus, agreement with the experiment, agreement between length and velocity, and agreement with other calculations all point to the accuracy of the present results.

The double maxima in the $2p$ cross section is more general than just the present He^- case. For *all* negative ions with outer np electrons, the εs continuum wave will be more penetrating than the corresponding εd. Thus, we predict that a photodetachment cross section with a two maxima, a sharp εs maximum close to threshold, and a broader εd maximum at higher energy, will generally occur for negative ions with outer np subshells, although depending upon the relative strengths and separation of the maxima, the total may show up as a maximum with a shoulder. This prediction is borne out in the limited number of extant cases [34]. More generally, for exactly the same reasons as the np photodetachment case, we expect the double maxima to occur for the photodetachment of all outer subshells with nonzero orbital angular momentum.

The photoelectron angular distribution asymmetry parameter, β, is shown in Fig. 4 in both length and velocity formulations which are in excellent agreement. For this case, at the MCHF level of approximation, β reduces to the Cooper-Zare formula [26],

$$\beta(2p) = \frac{2R_{\varepsilon d}^2 - 4R_{\varepsilon s}R_{\varepsilon d}\cos(\delta_{\varepsilon d} - \delta_{\varepsilon s})}{R_{\varepsilon s}^2 + 2R_{\varepsilon d}^2}, \qquad (5)$$

where $R_{\varepsilon s} = M(^4S)$ and $R_{\varepsilon d} = M(^4D)$. Looking at Fig. 4, it is seen that $\beta(2p)$ is zero at threshold, drops down to -1 just above threshold, then increases steadily to a value of about 1.6, followed by a slow steady decline. To understand this behavior, note that it has been found that, very near threshold, $R_{\varepsilon s} \gg R_{\varepsilon d}$. Defining $\eta = R_{\varepsilon d}/R_{\varepsilon s}$, and $\Delta = \delta_{\varepsilon d} - \delta_{\varepsilon s}$, Eq. (5) becomes,

$$\beta(2p) = \frac{2\eta^2 - 4\eta\cos\Delta}{1 + 2\eta^2}. \qquad (6)$$

As discussed above, near threshold $R_{\varepsilon d} \sim \varepsilon^{3/2}$, $R_{\varepsilon s} \sim \varepsilon^{1/2}$, so that $\eta \sim \varepsilon$. In addition, near threshold, $\Delta \approx -2\pi$, so that $\cos\Delta \approx 1$. Then, Eq. (6) shows that for small enough photoelectron energy, ε, $\beta(2p) \sim -4\varepsilon$, which shows that it vanishes as ε approaches zero, and goes rapidly negative with increasing ε. With further increases in ε, two things occur; $R_{\varepsilon d}$ increases rapidly, relative to $R_{\varepsilon s}$, and Δ begins to change significantly from the threshold value since $\delta_{\varepsilon d}$ increases and $\delta_{\varepsilon s}$ decreases, as seen in Fig. 2. Thus, $\cos\Delta$ decreases from unity and the η^2 term is no longer negligible in Eq. (6). The increase of the positive η^2 term, combined with the decrease of the negative second term causes $\beta(2p)$ to increase from -1 with increasing ε. Eventually $R_{\varepsilon d}$ dominates, as discussed above, and the $\cos\Delta$ term changes sign. These combine to increase in $\beta(2p)$ to its maximum value of about 1.6 in the vicinity of 4 eV. At this maximum value, $\cos\Delta \approx -1$. With further increase in energy, $\cos\Delta$ increases so that the second term in Eq. (6) is less positive, and a gradual decrease in $\beta(2p)$ ensues.

Also shown in Fig. 4 are experimental results from several reports of one group [11,12] which are in general agreement with our result. There appears to be some structure in the experimental curve at about 2.25 eV. We can find no theoretical evidence of any sort of structure in this region. Preliminary indications from a multichannel R-matrix calculation [35] gives no indication of this structure either. Furthermore, our results are in excellent agreement with a pre-

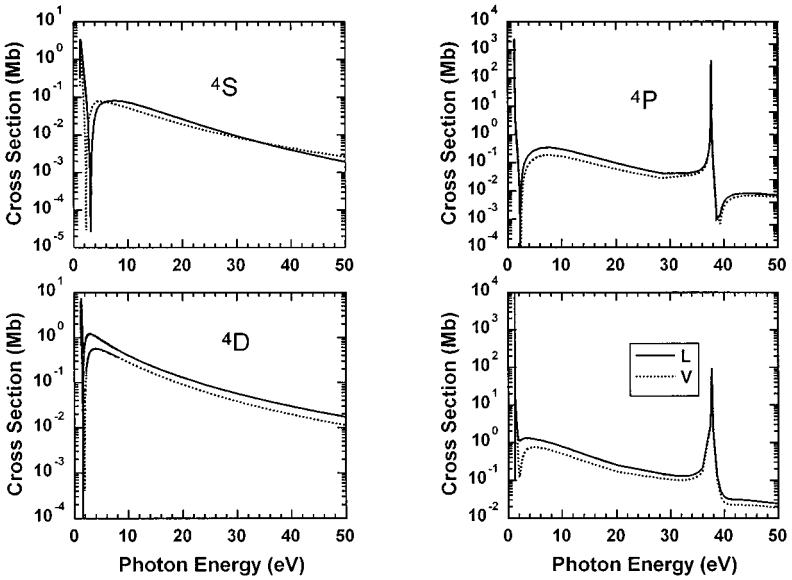

FIG. 5. Calculated $1s2s2p\ ^4P \rightarrow 1s2p\varepsilon p\ ^4S$, ^4P, and ^4D partial photodetachment cross sections along with their sum, the total $1s2s2p\ ^4P \rightarrow 1s2p\ ^3P$ cross section in dipole-length (L) and dipole-velocity (V) formulations.

vious MCHF calculation [18] which also shows no structure in this region. Thus it is felt that the measurements should be reconsidered.

B. Photodetachment of the 2*s* electron: The $1s2p\ ^3P$ He channel

In this case, the cross section is the sum of the $1s2s2p\ ^4P \rightarrow 1s2p\varepsilon p\ ^4S$, ^4P, and ^4D partial cross sections, each of which is shown in Fig. 5. Here it is seen that all three of the partial cross sections have Cooper minima just above threshold. The ^4S and ^4D channels have maxima just below the Cooper minima of about 4 Mb and 8 Mb, respectively, and falloff monotonically above the threshold region. The ^4P channel is decidedly different; there is a very strong resonance just above threshold, and another at about 38 eV. The fundamental difference between the ^4P channel, on the one hand, and the ^4S and ^4D on the other, is the existence of the $1s2p^2\ ^4P$ and $2s2p^2\ ^4P$ autodetaching states; they have no analogues with ^4S or ^4D symmetries. Thus, the ^4P partial cross section is qualitatively, as well as quantitatively, different from the ^4S and ^4D channels; however, away from the resonances, it is seen from Figs. 5 that all three channels are, in fact, quite similar. Note further that length and velocity are in relatively good agreement.

As in the case of $2p$ ejection, the behavior of these partial cross sections is determined primarily by a small number of terms in the corresponding matrix element. As a matter of fact, if we ignore the ^4P resonances for the moment, the dominant term in all three matrix elements can be characterized as

$$M(^4L) = \alpha_1 \langle 1s_i 2s_i 2p_i\ ^4P | D | 1s_f 2p_f \varepsilon p\ ^4L \rangle, \qquad (7)$$

where $L = S$, P, and D. Only this term is important because $\langle 2p_i | 2p_f \rangle$ is 0.99, while $\langle 3p_i | 2p_f \rangle$ is only -0.038. Thus, aside from overlap and angular factors, these matrix elements are essentially the single-particle matrix elements between $2s_i$ the various εp corresponding to the three different final-state angular-momentum couplings. The phase shifts, which characterize the continuum waves, are shown in Fig. 6, where it is seen that the ^4S and ^4D are very similar; both start at a value of π at threshold and dropping monotonically with increasing energy. But the ^4S phase shift remains a bit larger than the ^4D above threshold. The situation for ^4P is rather different owing to the resonances just above threshold and around 38 eV. These resonances cause the ^4P phase shift to have a value of $\pi/2$ at threshold, and a rapid increase from threshold, along with the structure at about 38 eV. Aside from the resonance effects, the ^4P phase shift is seen to be rather similar to the other two. Thus, away from the resonances, all three continuum waves are rather similar so that the radial parts of the matrix elements are also rather similar. Since the square of the angular integrals are in a ratio of 1:3:5 in order to ascending L, the cross sections should also reflect that ratio; Fig. 5 confirms that indeed they do, away from the resonances.

Since we are dealing with a negative ion, there is no necessity for Rydberg resonances below each threshold. In fact, there are none below the $2s$ detachment channel. The resonance that lies just above threshold is the $1s2p^2\ ^4P$ resonance that has been studied in some detail, both theoretically

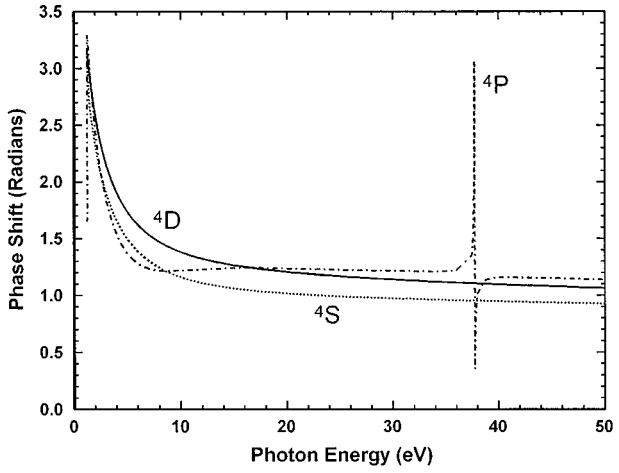

FIG. 6. Phase shifts for the $1s2p\varepsilon p\ ^4S$, ^4P, and ^4D final continuum states in He^-.

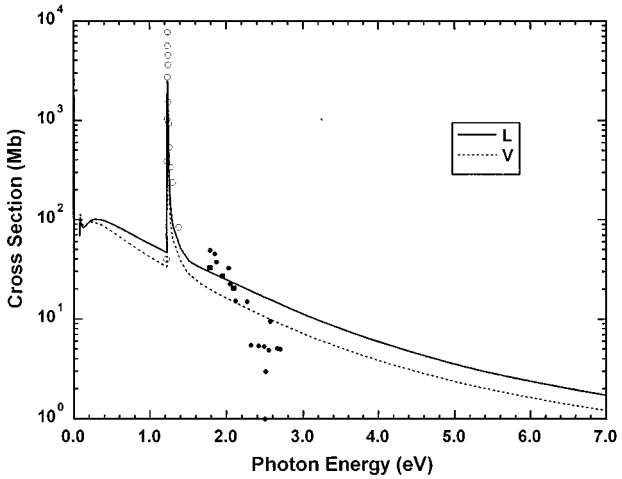

FIG. 7. Total photodetachment cross section for the $1s2s2p\ ^4P$ state of He^- in dipole-length (L) and dipole-velocity (V) formulations. The experimental points are from Ref. [7] [solid dots], Ref. [10] [open circles], and Ref. [11] [solid squares].

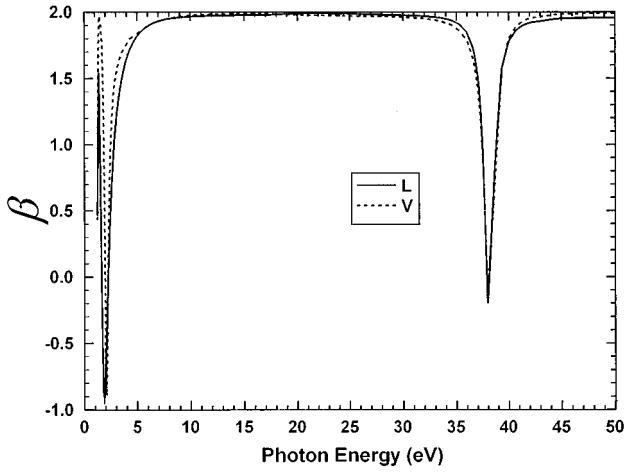

FIG. 8. Photoelectron angular distribution asymmetry parameter, β, for the $1s2s2p\ ^4P \rightarrow 1s2p\ ^3P$ photodetachment process in dipole-length (L) and dipole-velocity (V) formulations.

[14–18] and experimentally [8–10,13]. Since it lies above the $2s$ threshold it is called a shape resonance. We find the resonance at a photon energy of 1.234 eV, just 12.37 meV above the $2s$ threshold, and a width of 9.48 meV. These results compare favorably with earlier theoretical works [14–18] and, more importantly, with the latest high-resolution measurement of this resonance [13] which found it at 10.80 meV above the $2s$ threshold with a width of 7.16 meV. The higher-energy resonance is the $2s2p^2\ ^4P$ resonance. The resonance position found, at $h\nu = 37.683$ eV, is in excellent agreement with previous theoretical results of 37.671 eV [20,21] and 37.672 eV [22]. The width found, $\Gamma = 9.22$ eV, is also in reasonable agreement with previous values of 10.4 eV [20,21] and 9.87 eV [22]. Furthermore, we find an oscillator strength in this resonance transition of 0.109 in the length formulation and 0.106 in velocity, which compares favorably with the previous value of 0.100 [22]. Unfortunately, there is no experimental scrutiny of this resonance as yet.

This resonance is an example of a hollow negative-ion state since it contains all $n = 2$ electrons with an empty $n = 1$ shell; these states in neutral atoms, particularly Li, have been the subject of much recent scrutiny [36]. In the photoionization of ground-state neutral atoms, however, they tend to be small blips on a large nonresonant background [36]. The $2s2p^2$ resonance in He^-, on the other hand, dominates the photodetachment cross section, as seen in Figs. 5. The reason for this difference is that the $1s2s2p \rightarrow 2s2p^2$ transition in He^- is a one-electron transition and, thereby, quite strong. In studies of the photoionization of ground-state atoms, on the other hand, these hollow states can be reached only by two-electron transitions.

Of particular interest in connection with these resonances is that the $2s2p^2\ ^4P$ lies 1.034 eV *below* the $1s$ detachment threshold; a Rydberg resonance. The corresponding resonance in the vicinity of the $2s$ detachment threshold, $1s2p^2\ ^4P$, was seen to lie *above* the $2s$ threshold, a shape resonance. The difference in the character of the two resonances, i.e., why the $2s2p\ ^3P$ state of He has a significant electron affinity while the $1s2p\ ^3P$ state does not, is quite subtle. To begin with, the addition of a $2p$ electron to the $1s2p\ ^3P$ state of He leaves the $1s$ pretty much unchanged, but the $2p$ much more diffuse, owing to the mutual screening of the two $2p$ electrons in the $1s2p^2\ ^4P$ state of He^-. Aside from exchange, this leads to and increase in binding due to the binding of the extra $2p$ electron, but a decrease because each of the diffuse $2p$ electrons has a smaller screened nuclear binding along with the mutual repulsion of the $2p$ electrons. MCHF calculations show that these effects nearly cancel. Thus, the difference in binding energies between $1s2p\ ^3P$ and $1s2p^2\ ^4P$ results from the difference in $1s$–$2p$ exchange interactions. In both cases exchange is attractive, but it is significantly larger in the $1s2p\ ^3P$ state because the overlap of the $1s$ and $2p$ orbitals is much greater there than in the $1s2p^2\ ^4P$ case where the $2p$ orbitals are much more diffuse; this despite the fact that there are two $2p$ electrons in the latter case.

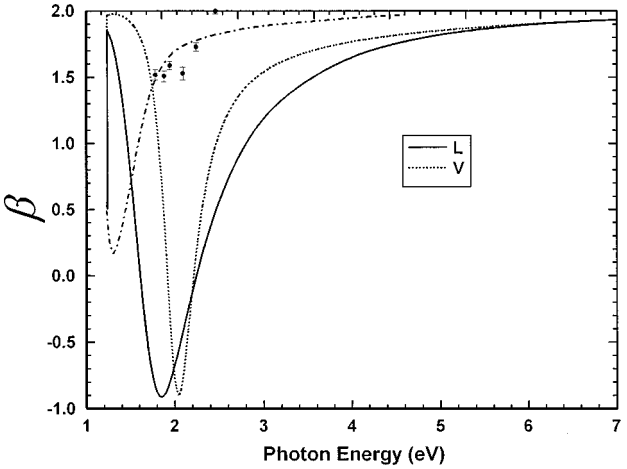

FIG. 9. Photoelectron angular distribution asymmetry parameter, β, for the $1s2s2p\ ^4P \rightarrow 1s2p\ ^3P$ photodetachment process in dipole-length (L) and dipole-velocity (V) formulations. The experimental points are from Refs. [11] and [12] and the dotted-dashed curve is the theoretical result of Ref. [18].

For the addition of a $2p$ electron to the $2s2p\ ^3P$ state of He to form the $2s2p^2\ ^4P$ state of He^-, the situation is similar to the previous case, with one important exception; here both electrons of the $2s2p\ ^3P$ state of He expand because of the mutual screening of all three $n=3$ electrons. Without exchange, the energies of the two states would be remarkably similar, as in the previous case, because of the approximate cancellation between the addition of the attractive force on the added electron combined with the decrease in nuclear attraction due to the increased size of the orbitals and the mutual repulsion of the electrons. Since all electrons in both states are $n=2$, however, the $2s$ and $2p$ orbitals occupy the same region of space in both the $2s2p\ ^3P$ state of He and the $2s2p^2\ ^4P$ state of He^-, although this region is more diffuse in He^-. Thus, the $2s-2p$ exchange interaction are large (and attractive) in both states; the fact that there are two $2p$ electrons in the $2s2p^2\ ^4P$ state causes the He^- attractive exchange interaction to be much larger than in the $2s2p\ ^3P$ state of He, thereby causing binding relative to the $2s2p\ ^3P$ state of neutral He and makes the $2s2p^2\ ^4P$ discrete state a Rydberg (Feshbach) resonance.

A comparison between the calculation and available experiment [7,10,11] is shown in Fig. 7. Above the opening of the $1s2p\ ^3P$ channel, only the total photodetachment cross section has been measured, so it is the total cross section shown in Fig. 7. From this comparison, it is seen that agreement is quite good overall, for both the resonant and the nonresonant cross section, except for the region around 2.5 eV, where experiment indicates some structure that we, along with previous calculations [15–18], do not predict. The overall agreement with experiment, however, gives us confidence that the calculated results will be of similar accuracy in energy regions where no experiment exists to check them.

Owing to the resonances and the Cooper minima, the photoelectron angular distribution asymmetry parameter, β, exhibits considerable structure, as seen in Fig. 8; there is considerable structure in the threshold region as well as in the 38 eV region. Away from these two energy regions, $\beta(2s)$ tends to 2. To understand this behavior, it is helpful to scrutinize the expression for $\beta(2s)$, which can be derived using the angular-momentum transfer analysis [26]

$$\beta(2s)=\frac{3R_1^2+7R_2^2+18R_1R_2\cos(\delta_1-\delta_2)+8R_2R_0\cos(\delta_2-\delta_0)}{2R_0^2+6R_1^2+10R_2^2}, \tag{8}$$

where $R_L=M(^4L)$ and δ_L is the associated phase shift. From this expression it is clear that if all of the matrix elements and phase shifts are equal, $\beta(2s)=2$. In the regions of the resonances, there are dramatic variations in R_1 and δ_1, as was seen above. In addition, in the threshold region there are extra variations associated with the Cooper minima in each of the matrix elements; the minima being at slightly different energies leads to a value of $\beta(2s)$ of -1 somewhere between the minima [26], just as seen in Fig. 8. Looking at the threshold region in more detail in Fig. 9, it is seen that there is some difference between length and velocity predictions, primarily due to slight differences in the location of the Cooper minima in the two formulations. Owing to the resonance, R_2 dominates at threshold; Eq. (8) shows that $\beta(2s)=0.5$ in such a circumstance, and that is seen in Fig. 9. Above the threshold resonance, all channels have appreciable amplitude and β tends towards 2, until the effects of the Cooper minima cause the pronounced dip, as seen, followed by a gradual rise back to 2 as the effect of the minima diminishes.

Also shown in Fig. 9 are the experimental results [11,12] which are not in very good agreement with our results; the experimental results appear to be shifted to the right from ours, possibly indicating at least one of the theoretical Cooper minima is at too low an energy. As a matter of fact, omission of interchannel coupling could have a significant effect on $\beta(2s)$, since the location of Cooper minima are extremely sensitive to interchannel coupling. In this case, the ^4D and ^4S channels arising from $2s$ detachment are degenerate with those from $2p$ detachment. Furthermore, the $2p$ channel cross sections are considerable larger than the corresponding $2s$ cross sections in the vicinity of the Cooper minima. At a photon energy of 5 eV, for example, the $2p\ ^4D$ cross section is about an order of magnitude larger than the $2s$, as can be seen from comparison of Figs. 1 and 5; a similar dominance, but not quite so pronounced, exists in the ^4S channel as well. Thus, owing to a degenerate channel of much larger strength, it is quite likely that the Cooper minima in the $2s\ ^4D$ and ^4S channels are significantly altered (or negated) by interchannel coupling. The ^4P channel, on the other hand, is not degenerate with any other channel, nor is there any strong channel close by. Thus it is unlikely that there would be a significant change in the Cooper minimum in this channel via interchannel coupling. Preliminary work including interchannel coupling and valence shell detachment plus excitation [35] bears out these ideas.

In addition, in Fig. 9 are the results of a previous MCHF calculation [18] which should closely resemble our results. The difference is, however, seen to be very great. We have tried to reproduce this calculation but were unable to get the same results.

C. Photodetachment of the 1*s* electron

For the ''main'' $1s$ photodetachment channel leading to the $2s2p\ ^3P$ autoionizing state of the He atom, the possible transitions are $1s2s2p\ ^4P\rightarrow 2s2p\varepsilon p\ ^4S$, ^4P, and ^4D, exactly the same as for the $2s$ photodetachment discussed above with $1s$ and $2s$ interchanged. The total cross section for this ''main'' channel, the sum of the three partial cross sections, is shown in Fig. 10 where a rise from threshold to a maximum of about 30 Mb, followed by a monotone decrease, is seen; no structure appears in this cross section. The dynamics of each of the transitions making up this cross

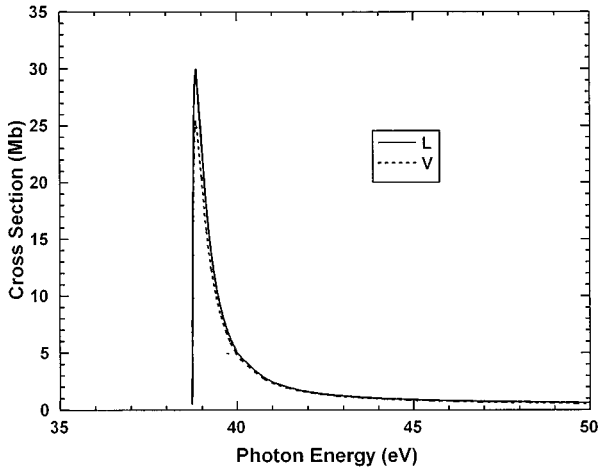

FIG. 10. Photodetachment cross section for the $1s2s2p\ ^4P \rightarrow 2s2p\ ^3P$ ''main'' channel in dipole-length (L) and dipole-velocity (V) formulations.

section is essentially the same; thus, the partial cross sections for the ^4S, ^4P, and ^4D transitions are almost exactly 1/9, 3/9, and 5/9 of the total.

The striking feature of this cross section is its maximum value. Since photodetachment cross sections *must* be zero at threshold [1], a maximum above threshold is inevitable. But, although the $1s$ orbital in this He^- state is virtually unscreened and quite similar to the $1s$ of He^+, the maximum in the $1s$ photodetachment cross section of about 30 Mb is much larger than is ever seen for *nonresonant* $1s$ photoionization of He^+ or any neutral atom; He has the highest at about 7 Mb at the ionization threshold [3]. Also seen is a much more rapid falloff with energy, as compared to neutral atoms [3]. Thus, the maximum in the photodetachment cross section just above threshold is more than a factor or four larger than the largest $1s$ photoionization cross section for any atom in the periodic table. To understand this behavior, note that the dominant terms in the matrix element for each transition in this ''main'' $1s$ cross section are given by

$$M(^4L) = \alpha_1 \langle 1s_i 2s_i 2p_i\ ^4P | D | 2s_f 2p_f \varepsilon p\ ^4L \rangle + \alpha_2 \langle 1s_i 2s_i 3p_i\ ^4P | D | 2s_f 2p_f \varepsilon p\ ^4L \rangle, \quad (9)$$

which is rather different from the $2s$ case. There are other major differences from $2s$ detachment in that the removal of the inner shell $1s$ electron causes significant relaxation of the final state $2s_f$ and, particularly, the $2p_f$ orbitals with respect to their initial-state counterparts [37]. Owing to this relaxation, $\langle 2p_i | 2p_f \rangle$ is 0.856, and the εp orbital, which is orthogonal to $2p_i$, has a significant overlap with $2p_i$ and $3p_i$ in the threshold region. Thus the major contributions to the matrix elements in the threshold region arise from terms proportional to

$$\langle 2s_i | 2s_f \rangle \langle 2p_i | \varepsilon p \rangle \langle 1s_i | D | 2p_f \rangle \quad (10)$$

and

$$\langle 2s_i | 2s_f \rangle \langle 3p_i | \varepsilon p \rangle \langle 1s_i | D | 2p_f \rangle \quad (11)$$

in which the energy dependence comes from the $\langle 2p_i | \varepsilon p \rangle$ and $\langle 3p_i | \varepsilon p \rangle$ terms. While both terms are important in the matrix element, the term associated with Eq. (11) is actually the larger of the two by a factor of 2 in the threshold region, despite the fact that the weight of the other term is greater by a factor of 2. This is because $\langle 2p_i | \varepsilon p \rangle$ has a maximum value of about 1.04, while $\langle 3p_i | \varepsilon p \rangle$ reaches 4.87. Note that these terms are negligible in the $2s$ detachment case since relaxation is unimportant there so that the εp orbital is nearly orthogonal to the $2p_i$ and $3p_i$ orbitals. Thus, the sharp maximum in the threshold region is a result of core relaxation; a relaxation spike.

Above threshold, the εp orbital moves in very rapidly with energy so that the overlaps, $\langle 2p_i | \varepsilon p \rangle$ and $\langle 3p_i | \varepsilon p \rangle$, in turn, diminish very rapidly, leading to the steep decline of the cross section shown in Fig. 10; this rapid dropoff is very uncharacteristic of photoabsorption by $1s$ electrons [3]. A few eV above the $1s$ threshold, these terms [Eqs. (10), (11)] are no longer the dominant part of the matrix elements; here the major contribution arises from terms of the form

$$\langle 2s_i | 2s_f \rangle \langle 2p_i | 2p_f \rangle \langle 1s_i | D | \varepsilon p \rangle, \quad (12)$$

which makes the $1s$ cross section anomalously small owing to the relaxation effect on the overlaps [37]. But if the strength of the $1s$ ''main'' cross section is diminished by overlap (relaxation) effects, this missing strength must go into detachment plus excitation.

To investigate this point, ''satellite'' processes consisting of the $1s$ photodetachment leaving the He in more highly excited autoionizing $2s2p\ ^3P$ state have been considered, i.e., detachment of the $1s$ electron along with excitation of one or both of the outer electrons. The ''satellite'' processes where the He atom is left in the nearly degenerate $\{2s3p \pm 3s2p\}\ ^3P$ states, also termed $(sp23\pm)\ ^3P$, were investigated. In these cases, the state designation is written in this way to emphasize that the excited state of He is roughly a 50-50 admixture of the two configurations. There are two such admixtures and the ''+'' designates the state where the coefficients of the two terms have the same sign, while in the ''−'' case, the coefficients are of the opposite sign. The transitions $1s2s2p\ ^4P \rightarrow (23sp\pm)\varepsilon p\ ^4S$, ^4P, and ^4D, were considered and the results for the total channel cross sections, summed in each case over the three multiplets, are shown in Fig. 11. Here we see a sharp spike just below 44 eV, which corresponds to the transition to the ''−'' state, and a much broader, though not quite as high, maximum with far more oscillator strength, resulting from the final ''+'' state. This is rather different from the strength of the analogous singlet states in photoabsorption from the ground state of He where, owing to cancellation, the ''+'' oscillator strength is roughly two orders of magnitude larger than the ''−'' [38].

To understand this, note that since the wave functions for the $(sp23\pm)\ ^3P$ states are considerably more complex than the $2s2p\ ^3P$ wave function, with two primary terms as discussed above, which leads to significant cancellation among various contributions to the dipole matrix elements. The weights of the $2s3p$ and $3s2p$ of the final ^3P states are, respectively, about 0.67 and 0.68 for the ''+'' state, and −0.54 and 0.69 for the ''−'' state, and we shall refer to

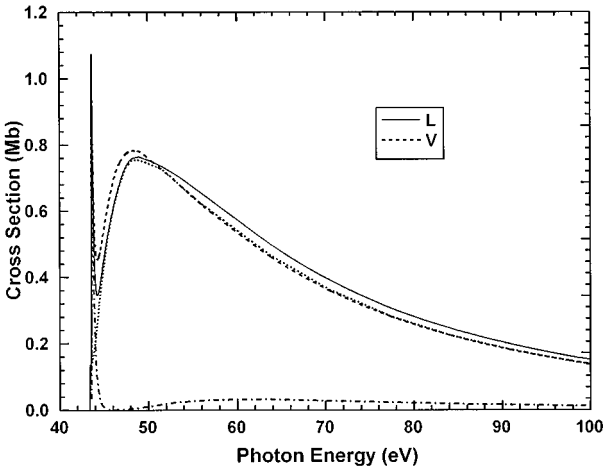

FIG. 11. Photodetachment cross section for the $1s2s2p\ ^4P \rightarrow (23sp+)\ ^3P$ [dots] and $1s2s2p\ ^4P \rightarrow (23sp-)\ ^3P$ [dotted-dashed] detachment plus excitation satellite channel in dipole-length formulation. The sum of these two cross sections is also shown in dipole-length (L) and dipole-velocity (V) formulations.

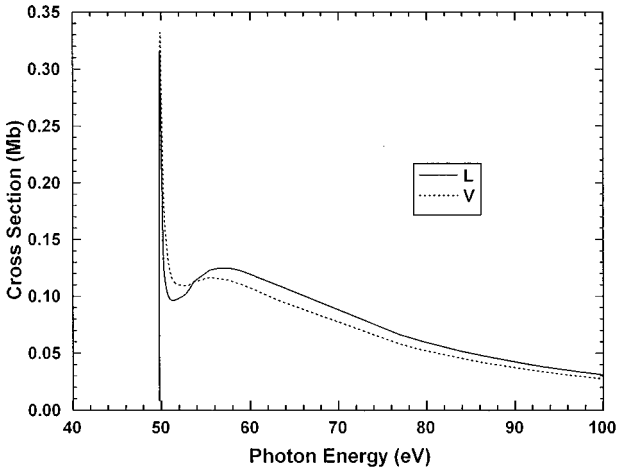

FIG. 12. Photodetachment cross section for the $1s2s2p\ ^4P \rightarrow 3s3p\ ^3P$ detachment plus excitation satellite channel in dipole-length (L) and dipole-velocity (V) formulations.

these coefficients as β_1 and β_2, respectively. Near threshold, there are six dominant terms for each transition ($^4S,P,D$) for both ''+'' and ''−'' cases and all include $\langle 2p_i|\varepsilon p\rangle$ and $\langle 3p_i|\varepsilon p\rangle$ overlaps which, as discussed above, are nonzero only because of relaxation and maximize just above threshold. These terms are of varying signs, leading to much cancellation in the dipole matrix elements. Owing to the fact that $\langle 2s_i|2s_f\rangle = 0.847$, while $\langle 2s_i|3s_f\rangle = -0.462$, the ''+'' dipole matrix element experiences almost total cancellation here because, as seen above, the coefficients of the two major terms in the final-state expansion, β_1 and β_2, are of the same sign. For the same reasons, the ''−'' dipole matrix element exhibits far less cancellation, leading to the relaxation spike seen just above threshold.

Away from threshold, since the $\langle 2p_i|\varepsilon p\rangle$ and $\langle 3p_i|\varepsilon p\rangle$ overlaps fall off very rapidly, the situation is different. Here the dominant terms involve only overlaps between initial and final discrete states which are not small owing to the significant relaxation to the removal of the $1s$ electron. Furthermore, in all important terms but one, they are of the same sign, so that here the cancellation of terms occurs in the ''−'' matrix element, not in the ''+''. This is evident in Fig. 11 where it is seen that, away from threshold, the ''+'' cross section dominates the ''−''. The increase of the ''+'' cross section from threshold, and subsequent falloff from the maximum, simply reflect the behavior of $\langle 1s_i|D|\varepsilon p\rangle$. The largeness of these detachment plus excitation cross sections, compared to the ''main'' transition, is a result of the size of the $\langle 2s_i|3s_f\rangle$ and $\langle 2p_i|3p_f\rangle$ overlaps relative to $\langle 2s_i|2s_f\rangle$ and $\langle 2p_i|2p_f\rangle$, respectively; they are all of the same order of magnitude owing to the ''collapse'' of the final-state orbitals in response to the removal of the $1s$ electron. Quantitatively, $\langle r\rangle$ for the initial state $n=2$ orbitals is about 5 a_0 (Bohr radii), while the final state $n=2$ and $n=3$ orbitals are less than 3 a_0 and about 9 a_0, respectively; the initial state $n=2$ orbitals occupy a region of space intermediate between the final state $n=2$ and $n=3$ orbitals.

This understanding of relaxation effects in the $1s2s2p\ ^4P \rightarrow (23sp\pm)\varepsilon p\ ^4S$, ^4P, and ^4D transitions suggests that transitions leaving the He atom in higher excited states in this series, $(2nsp\pm)\varepsilon p$ with $n>3$, will not be very important because the ns_f and np_f orbitals do not overlap the initial-state orbitals very well. These arguments also suggest that transitions leaving He in the $3s3p\ ^3P$ state will be of some importance. To leave He in this state the possible transitions are $1s2s2p\ ^4P \rightarrow 3s3p\varepsilon p\ ^4S$, ^4P, and ^4D; the calculated cross sections, summed over ^4S, ^4P, and ^4D are shown in Fig. 12, where a threshold spike is seen, followed a slight dip before the eventual falloff with increasing energy. The height of the spike is about 0.3 Mb and above the spike, the cross section has a maximum of only about 0.1 Mb. Although the shape of this $3s3p$ cross section is similar to the sum of the $23sp\pm$ results [Fig. 11], the explanation for the shape is rather similar to $2s2p$. Near threshold the dominant contributions to the dipole matrix element are terms just like Eqs. (10) and (11) for $2s2p$ with $2s_f$ and $2p_f$ replaced by $3s_f$ and $3p_f$, respectively,

$$\langle 2s_i|3s_f\rangle\langle 2p_i|\varepsilon p\rangle\langle 1s_i|D|3p_f\rangle \tag{13}$$

and

$$\langle 2s_i|3s_f\rangle\langle 3p_i|\varepsilon p\rangle\langle 1s_i|D|3p_f\rangle \tag{14}$$

in which the energy dependence is again seen to come entirely from the $\langle 2p_i|\varepsilon p\rangle$ and $\langle 3p_i|\varepsilon p\rangle$ terms. But the $\langle 2p_i|3p_f\rangle$ overlap of the $3s3p$ transition is more than a factor of 2 smaller than the $\langle 2p_i|2p_f\rangle$ of the $2s2p$, the $\langle 1s_i|D|3p_f\rangle$ matrix element is about a factor of 2.5 smaller than the corresponding $\langle 1s_i|D|2p_f\rangle$, the $\langle 2p_i|\varepsilon p\rangle$ and $\langle 3p_i|\varepsilon p\rangle$ are smaller for $3s3p$ than for $2s2p$ final states owing to the differences in the p in the two cases, and some further cancellation exists in the $3s3p$ case owing to the contribution of the $1s3s3p$ term in the initial-state expansion, a term which is much less important for $2s2p$. All of these effects combine to make the matrix element and order of magnitude smaller in the $3s3p$ case, as compared to the $2s2p$, so that the cross section is down by a factor of 100,

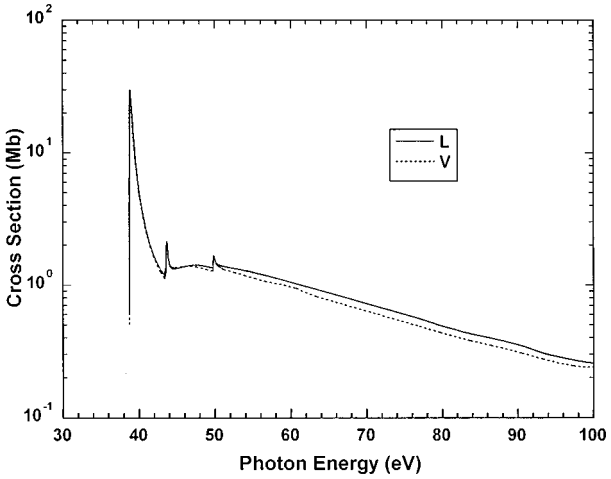

FIG. 13. Total $1s$ photodetachment cross section, summed over ''main'' and satellite channels, in dipole-length (L) and dipole-velocity (V) formulations.

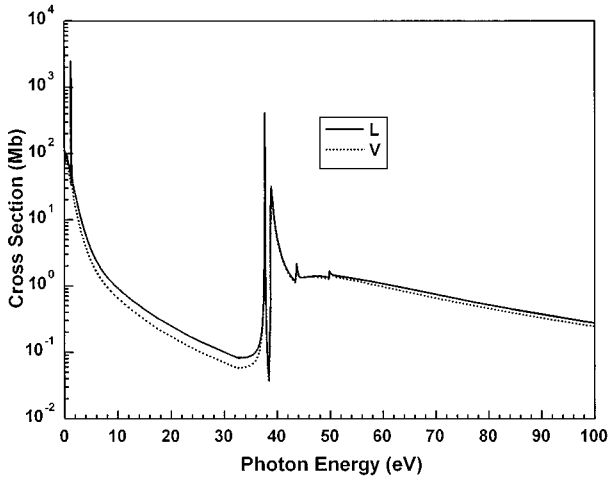

FIG. 14. Total photodetachment cross section for the $1s2s2p\ ^4P$ state of He^- in dipole-length (L) and dipole-velocity formulations.

0.3 Mb as opposed to 30 Mb as seen in Figs. 12 and 10, respectively. Away from threshold, the dominant term is the analogue of Eq. (12),

$$\langle 2s_i|3s_f\rangle\langle 2p_i|3p_f\rangle\langle 1s_i|D|\varepsilon p\rangle, \tag{15}$$

where $2s_f$ and $2p_f$ replaced by $3s_f$ and $3p_f$, respectively. In this case, the product of the overlaps, in this term is about a factor of 3 smaller than the product of $\langle 2s_i|2s_f\rangle$ and $\langle 2p_i|2p_f\rangle$ relevant to $2s2p$ [Eq. (12)] so that the cross section is about an order of magnitude smaller, as seen. The fact that the threshold relaxation spike is two orders of magnitude smaller in the $3s3p$ case, as opposed to the $2s2p$ means that it loses its strength much closer to threshold when the term proportional to Eq. (15) is still rising. This leads to the small dip between the two maxima for $3s3p$ which is not seen for $2s2p$ owing to the strength of the threshold relaxation spike.

The total $1s$ cross section, summed over the various final states considered, is given in Fig. 13. It is evident that near the $1s$ detachment threshold, the $2s2p\ ^3P$ channel relaxation spike dominates the $1s$ photodetachment cross section. Above the satellite threshold, this is clearly no longer the case; the satellite cross section dominate the total $1s$ detachment at the higher energies. In fact, above about 55 eV, the ''main'' $2s2p\ ^3P$ channel amounts to only about 1/3 of the $1s$ cross section, while the $(23sp+)\ ^3P$ channel is about 1/2, and the $3s3p\ ^3P$ is most of the rest; the $(23sp-)\ ^3P$ contribution is quite small everywhere except at the threshold relaxation spike. These ratios remain just about constant over the entire higher-energy range that we have investigated, and should continue asymptotically at the same values. Thus, away from the threshold relaxation spike in the ''main'' $2s2p\ ^3P$ channel, the $1s$ photodetachment cross section is dominated by detachment plus excitation owing to the relaxation effects of the removal of the $1s$ electron.

It is of interest to look at where the $1s$ oscillator strength goes. While the sum rule governing the total photoabsorption of the atom, the sum of all of the oscillator strength discrete and continuum equals the number of electrons (three in this case) is essentially exact [3], it is also generally *approximately* true subshell by subshell, at least to within 10–20 %. The oscillator strength in the $2s2p$ threshold relation peak up the opening of the $(23sp\pm)$ channels is 0.21, a factor of 2 larger than the 0.11 oscillator strength of the resonance lying just below the $1s$ detachment threshold. This emphasizes the difference in physical origin of the two peaks. The total in the $2s2p$ channel to 100 eV is found to be 0.40. For the other $1s$ channels considered, the oscillator strengths to 100 eV of $(23sp-)$, $(23sp+)$, and $3s3p$ are 0.015, 0.20, and 0.034, respectively. The total $1s$ oscillator strength, up to 100 eV, including the $1s\rightarrow 2p$ resonance transition, is, thus, 0.76. We estimate that the $1s$ oscillator strength lying above 100 eV is 0.15, giving an approximate $1s$ total oscillator strength of a bit over 0.9, well within the expectation of the one-electron sum rule.

Finally, note that for each of these $1s$ photodetachment channels the ^4S, ^4P, and ^4D matrix elements differ only by geometric (angular-momentum) factors, not by dynamics; the phase shifts of each of the ^4S, ^4P, and ^4D continuum waves within a given channel are almost exactly the same. As a result, the photoelectron angular distribution asymmetry parameter, β, is equal to 2 [26], independent of energy, obviating any reason to discuss it further.

D. Total cross section

The total cross section for photodetachment of the $1s2s2p\ ^4P$ state of He^- is shown in Fig. 14 for completeness where the relative magnitudes of the various features discussed above for the individual channels are clearly evident. Except for the 3–5 eV region, as noted earlier, where valence shell detachment plus excitation (along with the associated resonances) has not been considered, it is believed that this cross section should be reasonably accurate. The total oscillator strength to 100 eV is found to be 2.61; when we add the estimated oscillator strength above 100 eV of 0.15, as discussed above, we find a total above the first photodetachment threshold of 2.76. It is likely that the remaining 0.24 lies in the discrete $2p$ excitations.

IV. CONCLUDING REMARKS

Multiconfiguration Hartree-Fock (MCHF) calculations of the photodetachment of the $1s2s2p\ ^4P$ metastable state of

He^- have been presented from the detachment threshold to a photon energy of 100 eV. In addition, resonance phenomena were included by explicitly introducing interchannel coupling. For the valence shell photodetachment, general agreement was found with previous work, both experimental and theoretical. Some differences with experiment, likely due to neglecting interchannel coupling of weak open channels degenerate with strong ones were pointed out. Work including this coupling is in progress [35].

The primary focus of this work, however, was the photodetachment of the $1s$ electron where it was found that the relaxation of the core, in response to $1s$ electron removal, causes a variety of phenomena including threshold relaxation spikes at the onset of the $1s$ detachment channels, a huge *nonresonant* $1s$ cross section, and the dominance of detachment plus excitation from a little way above the $1s$ detachment threshold to very high energy. We note, however, that the omission of interchannel coupling between continuum channels, along with out neglect of a host of other ''hollow'' resonances, could alter the details of some of the results presented. No experimental investigation of the photodetachment He^- in the vicinity of the $1s$ detachment threshold exists, although the technology to produce to He^- certainly exists, as evidenced by the experimental activity on valence shell photodetachment [7–13], and third generation synchrotron light sources exist with high brightness in the relevant energy region.

The cross section for the hollow ion Feshbach resonance, $2s2p^2\ ^4P$, just below the $1s$ detachment threshold, was also scrutinized for the first time. It was found to be so strong since, the transition is essentially a $1s \rightarrow 2p$ one-electron transition; transitions to other hollow states will also be significantly larger than their counterparts in ground state photoionization of Li owing to the fact that in the He^- case, the initial state contains two valence electrons.

In addition, it is useful to note that both the ''main'' $1s$ detachment, and the various detachments plus excitation, leave the He atom in an autoionizing state. Thus, the resulting autoionizing lines can be used as signatures to distinguish the processes experimentally. In addition, these are triplet autoionizing states which cannot be reached from the singlet ground state of He by photoabsorption. Thus the possibility of studying the triplet manifold experimentally in a ''cleaner'' and more unambiguous manner than via electron scattering.

Finally, the relaxation effects in $1s$ photodetachment should not be limited to He^-. While the details of the cross sections will surely differ, the physical interactions which lead to the $1s$ results in He^- should be equally strong in $1s$ photodetachment of any negative ion, e.g., threshold relaxation spikes, along with the dominance of detachment plus excitation at the higher energies, will be generally true for $1s$ photodetachment of any negative atomic ion, and similar types of effects should be found for negative molecular ions as well.

ACKNOWLEDGMENTS

This work was supported by NSF and NASA. Numerous discussions with C. F. Fischer through the initial phase of this work are gratefully acknowledged, along with an important discussion with P. L. Altick.

[1] *Applied Atomic Collision Physics*, edited by H. S. W. Massey, E. W. McDaniel, and B. Bederson (Academic, New York, 1983), 5 volumes.

[2] *Photoionization and Other Probes of Many-Electron Interactions*, Vol. 18 of *NATO Advanced Study Institutes Series B: Physics*, edited by F. J. Wuilleumier (Plenum, New York, 1976).

[3] J. Berkowitz, *Photoabsorption, Photoionization, and Photoelectron Spectroscopy* (Academic, New York, 1979).

[4] A. F. Starace, in *Handbuch der Physik*, edited by W. Mehlhorn (Springer-Verlag, Berlin, 1982), Vol. 31, pp. 1–121.

[5] *Many-Body Theory of Atomic Structure and Photoionization*, edited by T.-N. Chang (World Scientific, Singapore, 1993).

[6] R. Novick and D. Weinflasch, in *Precision Measurement and Fundamental Constants. NBS Special Publication No. 343*, edited by D. N. Lankenberg and B. N. Taylor (U.S. GPO, Washington, DC, 1971), pp. 403–410.

[7] R. N. Compton, G. D. Alton, and D. J. Pegg, J. Phys. B **13**, L651 (1980).

[8] R. V. Hodges, M. J. Coggiola, and J. R. Peterson, Phys. Rev. A **23**, 59 (1981).

[9] J. R. Peterson, M. J. Coggiola, and Y. K. Bae, Phys. Rev. Lett. **50**, 664 (1983).

[10] J. R. Peterson, Y. K. Bae, and D. L. Huestis, Phys. Rev. Lett. **55**, 692 (1985).

[11] D. J. Pegg, J. S. Thompson, J. Dellwo, R. N. Compton, and G. D. Alton, Phys. Rev. Lett. **64**, 279 (1990).

[12] J. S. Thompson, D. J. Pegg, R. N. Compton, and G. D. Alton, J. Phys. B **23**, L15 (1990).

[13] C. W. Walter, J. A. Seifert, and J. R. Peterson, Phys. Rev. A **50**, 2257 (1994).

[14] C. A. Nicolaides, Y. Komninos, and D. R. Beck, Phys. Rev. A **24**, 1103 (1981).

[15] A. U. Hazi and K. J. Reed, Phys. Rev. A **24**, 2269 (1981).

[16] S. Watanabe, Phys. Rev. A **25**, 2074 (1982).

[17] L. V. Chernysheva, G. F. Gribakin, V. K. Ivanov, and M. Yu. Kuchiev, J. Phys. B **21**, L419 (1988).

[18] H. P. Saha and R. N. Compton, Phys. Rev. Lett. **64**, 1510 (1990).

[19] M. Bylicki, Phys. Rev. A **45**, 2079 (1992).

[20] M. Bylicki and C. A. Nicolaides, Phys. Rev. A **48**, 3589 (1993).

[21] M. Bylicki and C. A. Nicolaides, Phys. Rev. A **51**, 204 (1995).

[22] K. T. Chung, Phys. Rev. A **51**, 844 (1995).

[23] C. F. Fischer, *The Hartree-Fock Method For Atoms* (Wiley-Interscience, New York, 1977).

[24] H. A. Bethe and E. E. Salpeter, *Quantum Mechanics of One- and Two-Electron Atoms* (Springer-Verlag, Berlin, 1957), pp. 248–252.

[25] C. N. Yang, Phys. Rev. **74**, 764 (1948).

[26] S. T. Manson and A. F. Starace, Rev. Mod. Phys. **54**, 389 (1982).
[27] C. F. Fischer, Comput. Phys. Commun. **64**, 369 (1991).
[28] A. V. Bunge and C. F. Bunge, Phys. Rev. A **30**, 2179 (1984).
[29] C. E. Moore, *Atomic Energy Levels*, Natl. Bur. Stand. (U.S.) Circ. No. 467 (U.S. GPO, Washington, D.C., 1949).
[30] K. T. Chung and I.-H. Chen, Phys. Rev. A **10**, 997 (1974).
[31] K. T. Chung and B. F. Davis, Phys. Rev. A **22**, 835 (1980) and references therein.
[32] Z. Felfli, Ph.D. thesis, Georgia State University, 1993 and (unpublished).
[33] U. Fano, Phys. Rev. **124**, 1806 (1961).
[34] V. K. Ivanov and L. P. Krukovskaya, J. Phys. B **27**, 4111 (1994) and references therein.
[35] H.-L. Zhou, F. Robicheaux, and S. T. Manson, Bull. Am. Phys. Soc. **40**, 1313 (1995); H.-L. Zhou, F. Robicheaux, D.-S. Kim, and S. T. Manson (unpublished).
[36] L. M. Kiernan, E. T. Kennedy, J.-P. Mosnier, J. T. Costello, and B. F. Sonntag, Phys. Rev. Lett. **72**, 2359 (1994).
[37] Z. Felfli and S. T. Manson, Phys. Rev. Lett. **68**, 1687 (1992).
[38] V. Schmidt, Rep. Prog. Phys. **55**, 1483 (1992) and references therein.